Aeroacoustic sources in turbulent flow through a pipe with a sharp orifice predicted by Large-Eddy Simulation

Johannes Tieber[1], Helfried Steiner[1], Paul Maurerlehner[2], Stefan Schoder[2], Manfred Kaltenbacher[2], Günter Brenn[1]

[1] *Institute of Fluid Mechanics and Heat Transfer, TU Graz, 8010 Graz, Austria, Email: helfried.steiner@tugraz.at*

[2] *Institute of Fundamentals and Theory in Electrical Engineering, TU Graz, 8010 Graz, Austria, Email: paul.maurerlehner@tugraz.at*

Abstract

The method of Large-Eddy Simulation (LES) has increasingly gained popularity, as it resolves a significant part of the vortical motion directly in a turbulent flow field. The uncertainty of turbulence modeling is thus limited to the unresolved sub-grid scales (SGS). This makes LES a highly attractive method for predicting flow-induced sound sources for use in Hybrid Computational Aero-acoustics (CAA). The possible sound emission generated by turbulent vortical motion is of growing importance in the design of flow-guiding components. This is especially the case in electric vehicles, where the masking noise of the combustion engine is absent, and limited space in the vehicle's engine compartment of the vehicle may lead to unfavorable flow conditions. The present study performs incompressible LES to predict the turbulent flow field of an orifice inside a straight circular pipe. The predicted instantaneous flow field is used to evaluate aeroacoustic source terms for different acoustic equations, such as Lighthill's wave equation or the Perturbed Convective Wave Equation (PCWE). The contribution of the unresolved scales, which is supplied to the acoustic sources by the employed SGS-model, is specially investigated. The computational results are also compared against experimental data from reliable measurements.

Introduction

The compressible conservation equations of fluid mechanics are basically able to describe all physically relevant phenomena of turbulent flow, as well as acoustic wave propagation. The difficulty of numerically resolving both phenomena lies in the large difference of the relevant length scales. On the one hand, the turbulent motion has to be resolved down to the smallest turbulent scales represented by the Kolmogorov scale. On the other hand, the much larger acoustic wavelengths need to be resolved as well. This disparity of scales makes a Direct Numerical Simulation (DNS) computationally unfeasible in most aeroacoustic problems. One possible remedy to this limitation is the so-called hybrid approach. For low Mach number applications, the turbulent flow field and the acoustic wave propagation can be split, thus computing the turbulent flow field and the flow-induced source terms separately from the wave propagation. The method of LES basically intends to resolve directly a major part of the turbulent motion, so that only the unresolved subgrid-scales (SGS) need to be modelled. As a result, the resolved aeroacoustic source terms predicted by LES can be regarded as a very accurate description without the often considerable uncertainties of statistical turbulence models.

In this study we apply the method of LES to a straight pipe ($D = 50\,\mathrm{mm}, Re_\mathrm{B} = 12650$), with an orifice obstructing the upper half cross section of the pipe, to predict aeroacoustic source terms for Lighthill's wave equation and the Perturbed Convective Wave Equation (PCWE). In case of Lighthill's wave equation, the SGS-contribution is considered and quantitatively examined as well. A special focus is on the flow phenomena appearing around the orifice and the dynamic structures responsible for the generation of flow-induced noise.

Governing equations

In the limit of isothermal low Mach number flow, the incompressible (fluid density $\rho = \rho_0 = \text{const.}$) balance equations of mass and momentum can be written as

$$\frac{\partial u_j}{\partial x_j} = 0 \text{ and } \frac{\partial u_i}{\partial t} + \frac{\partial u_i u_j}{\partial x_j} = -\frac{1}{\rho_0}\frac{\partial p}{\partial x_i} + \nu \frac{\partial^2 u_i}{\partial x_j \partial x_j}, \quad (1)$$

where u_i is the fluid velocity, ν is the kinematic viscosity and p is the pressure. Starting, on the other hand, from the fully compressible formulation, Lighthill's equation [1] provides a wave operator for the pressure fluctuations $p' = p - \langle p \rangle$ written as

$$\frac{1}{c_0^2}\frac{\partial^2 p'}{\partial t^2} - \frac{\partial^2 p'}{\partial x_i \partial x_j} = \frac{\partial^2 T_{ij}}{\partial x_i \partial x_j} \approx \rho_0 \frac{\partial}{\partial x_i}\left(\frac{\partial u_i u_j}{\partial x_j}\right), \quad (2)$$

where c_0 is the speed of sound and $p' = p_\mathrm{ic} + p_\mathrm{a}$ is a superposition of an incompressible and a compressible (acoustic) fluctuation. The righthand side represents the required source term, where $T_{ij} = \rho u_i u_j + \tau_{ij} + (p' - c_0^2 \rho')\delta_{ij}$ is the Lighthill stress tensor. For isothermal low Mach number flow, and neglecting viscous dissipation, the source term simplifies to the divergence of the advective momentum transport flux, as indicated on the rhs of equation (2). The PCWE [2] introduces a decomposition of the flow variables into a statistical average, an incompressible, and a compressible fluctuation, generally written as

$$\phi = \langle \phi \rangle + \phi_\mathrm{ic} + \phi_\mathrm{a}. \quad (3)$$

An acoustic potential ψ_a is further introduced, providing the acoustic velocity and pressure fluctuations as

$$u_{i,\mathrm{a}} = -\frac{\partial \psi_\mathrm{a}}{\partial x_i} \text{ and } p_\mathrm{a} = \rho_0 \frac{D\psi_\mathrm{a}}{Dt}, \quad (4)$$

respectively, with $D/Dt = \partial/\partial t + \langle u_j \rangle \, \partial/\partial x_j$. The acoustic potential is obtained in the PCWE by the solution of the following wave equation

$$\frac{1}{c_0^2}\frac{D^2\psi_\mathrm{a}}{Dt^2} - \frac{\partial^2\psi_\mathrm{a}}{\partial x_j \partial x_j} = -\frac{1}{\rho_0 c_0^2}\frac{Dp_\mathrm{ic}}{Dt}. \tag{5}$$

The rhs again represents a source term to be provided by the incompressible LES.

Simulation model and setup

The method of Large-Eddy Simulation (LES) by definition resolves only the large energy-carrying scales. In a mathematical sense, the method thus solves a spatially filtered representation of the Navier-Stokes equations defined in equation (1), written as

$$\frac{\partial \overline{u}_j}{\partial x_j} = 0 \text{ and} \tag{6}$$

$$\frac{\partial \overline{u}_i}{\partial t} + \frac{\partial \overline{u}_i \overline{u}_j}{\partial x_j} = -\frac{1}{\rho_0}\frac{\partial \overline{\pi}}{\partial x_i} + \nu \frac{\partial^2 \overline{u}_i}{\partial x_j^2} - \frac{\partial \tau_{ij,\mathrm{SGS}}}{\partial x_j}. \tag{7}$$

The overbars denote here the spatial filtering, generally defined as

$$\overline{\phi}(\vec{x}, t) = \int_\Omega \phi(\vec{\xi}) G(\vec{x} - \vec{\xi}; \bar{\Delta}) d\vec{\xi}, \tag{8}$$

involving the filter function G, dependent on the spatial distance $\vec{x} - \vec{\xi}$, and the filter width $\bar{\Delta}$. The stress tensor $\tau_{ij,\mathrm{SGS}} = \overline{u_i u_j} - \overline{u}_i \overline{u}_j$ represents the unresolved "subgrid" scales. Its deviatoric part is modelled using Boussinesq's eddy viscosity-based approach, written as

$$\tau_{ij,\mathrm{SGS}} - \tau_{kk,\mathrm{SGS}}\frac{\delta_{ij}}{3} = -2\nu_\mathrm{SGS}\overline{S}_{ij}, \tag{9}$$

where ν_SGS is the eddy-viscosity and $\overline{S}_{ij} = (\partial \overline{u}_i/\partial x_j + \partial \overline{u}_j/\partial x_i)/2$ is the resolved rate-of-strain tensor. The isotropic part of $\tau_{ij,\mathrm{SGS}}$ is absorbed into the so-called pseudo pressure $\overline{\pi} = \overline{p} - \tau_{kk,\mathrm{SGS}}\delta_{ij}/3$. In the present study, the eddy viscosity is obtained with the Coherent Structure Model (CSM) [3] as

$$\nu_\mathrm{SGS} = C\Delta^2 |\overline{S}_{ij}| \text{ and } C = \frac{1}{22}|F_\mathrm{CS}|^{3/2}(1 - F_\mathrm{CS}), \tag{10}$$

where Δ is the cubic root of the local cell volume, representing the computational mesh size. The Coherent Structure function is defined as

$$F_\mathrm{CS} = -\left(\frac{\partial \overline{u}_i}{\partial x_j}\frac{\partial \overline{u}_j}{\partial x_i}\right) \Big/ \left(\frac{\partial \overline{u}_j}{\partial x_i}\frac{\partial \overline{u}_j}{\partial x_i}\right). \tag{11}$$

Simulation setup

The investivated geometry is a straight circular pipe with diameter $D = 50\,\mathrm{mm}$, with a half moon-shaped orifice obstructing the upper half of the cross section (see figure 1). The entire domain is $25D$ long, with a $5D$ long inlet section upstream of the orifice. At solid walls, the no-slip boundary condition (BC) was applied, while on the outlet face, $20D$ downstream of the orifice, an averaged pressure BC was applied. The turbulent inflow

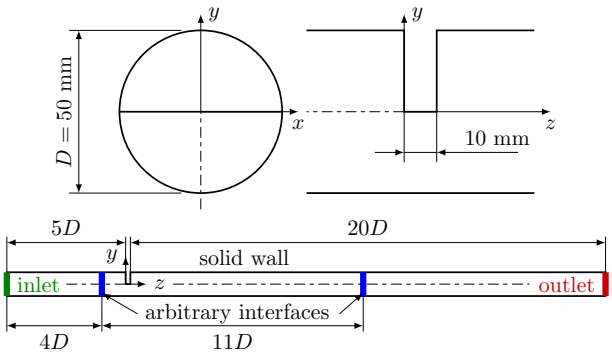

Figure 1: Upper subfigures: front and side views of the orifice obstructing the upper half of the cross section. Bottom subfigure: full computational domain.

BC was generated using an LES solution of fully developed pipe flow, where the instantaneous velocity distribution obtained on a given cross section was conservatively mapped to the inlet boundary of the pipe flow configuration with the orifice. The investigated flow is specified by the wall friction Reynolds number of the inflow, $Re_\tau = Du_\tau/\nu = 750$, where the wall shear stress based velocity is $u_\tau = \sqrt{(\tau_\mathrm{W}/\rho)}$. The corresponding bulk Reynolds number $Re_\mathrm{B} = Du_\mathrm{B}/\nu \approx 12650$, using the volumetric flow rate-equivalent "bulk" velocity u_B as the velocity scale. Near the orifice, the spatial discretization was refined. The highly refined section is connected with coarser discretized sections up- and downsteam using arbitrary interfaces, as depicted in figure 1, bottom. After having reached statistical convergence, the aeroacoustic source terms were recorded over an interval of $\Delta T = 0.2s$. A small time step $\Delta t = 1E^-5s$ was used to ensure a CFL number ~ 1 even in the highly refined region of the mesh around the orifice.

Simulation results

Figure 2 shows the contours of the instantaneous axial velocity near the orifice on the meridional plane of symmetry. Due to the blockage of the upper part of the cross section, the flow is accelerated, redirected downwards, and passed through the lower open part of the constriction at high velocity. In the separated flow region downstream of the orifice, a large recirculation zone is formed, which axially extends to the reattachment point at roughly $z_\mathrm{RP} \sim 0.185\,\mathrm{m} = 3.7D$. Multiple secondary recirculation zones right below the orifice and in the corners up- and downstream of the orifice are observed as well, as seen in the enlargened view in figure 2 c. The reattachment point is not stationary, but oscillates around a certain mean position. This particular feature was also reported in planar flow over a backward-facing step, which exhibits a similar large detached flow region caused by a step-like change in cross section, as exemplarily sketched in figure 3 a. Spazzini et. al. [4], who experimentally investigated such a generic flow configuration, found the spatial oscillation of the reattachement point to be associated with a dimensionless Strouhal number $Sr_\mathrm{RP} = fL_\mathrm{ref}/u_\mathrm{ref} \sim 1$, using the reattachment length, L_ref, and the inflow bulk velocity upstream of the step, u_ref, as the reference scales. The time signals of the pre-

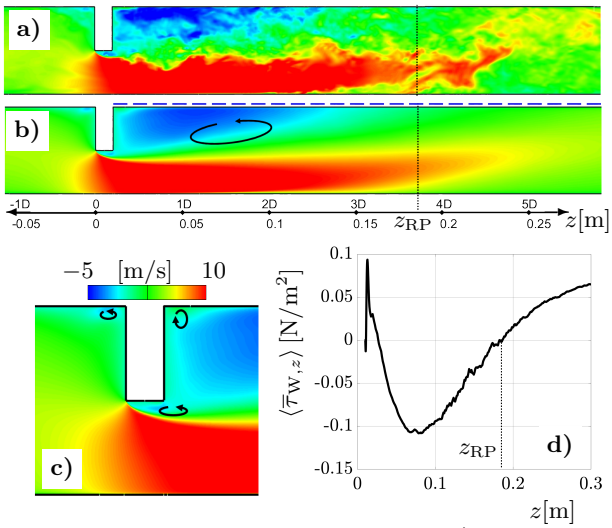

Figure 2: Contours of axial velocity $\overline{u}_z$: a) instantaneous field, b) averaged field $\langle\overline{u}_z\rangle$, c) enlarged view of region near the orifice, indicating secondary rezirculation zones. d) variation of averaged axial wall shear stress $\langle\overline{\tau}_{W,z}\rangle$ along top wall downstream of the orifice. The position of the reattachment point z_{RP} is always marked by a vertical dotted line.

dicted wall shear stress $\overline{\tau}_{W,z}$ near the reattachment point shown in figure 3 b clearly reflect this low-frequency oscillation. Applying a spectral analysis, and rescaling the frequency to a Strouhal number $Sr_{RP} = f z_{RP}/(2u_B)$, makes evident that the highest amplitudes appear around $Sr_{RP} \sim 1$ also in the present configuration, as seen from figure 3 c. A large part of the flow-induced noise is expected to be generated by the vortices, shed from the upstream edge of the orifice. The centers of these vortices can be identified as local minima of the incompressible pseudo pressure fluctuation $\overline{\pi}_{ic}$, as depicted in figure 4 a. Time signals of the pseudo pressure fluctuations $\overline{\pi}_{ic}$, recorded at three selected positions, are shown in figure 4 b. The variations show a shedding frequency of approximately $f = 1/\Delta t_{\pi,\min} \approx 100$ Hz. The spectral analysis shown in figure 4 c accordingly indicates high broadband amplitudes around approximately 100 Hz.

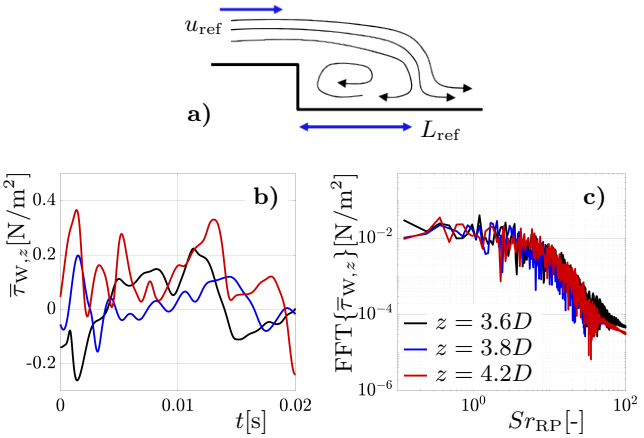

Figure 3: a) Flow over a planar backward facing step studied in [4], b) time signals of axial wall shear stress $\overline{\tau}_{W,z}$ at three positions near the reattachment point, c) spectral representation.

The high vorticity in the shear layer downstream of the orifice leads to high turbulent kinetic energy $\overline{k} = \overline{u}_i'\overline{u}_i'/2$,

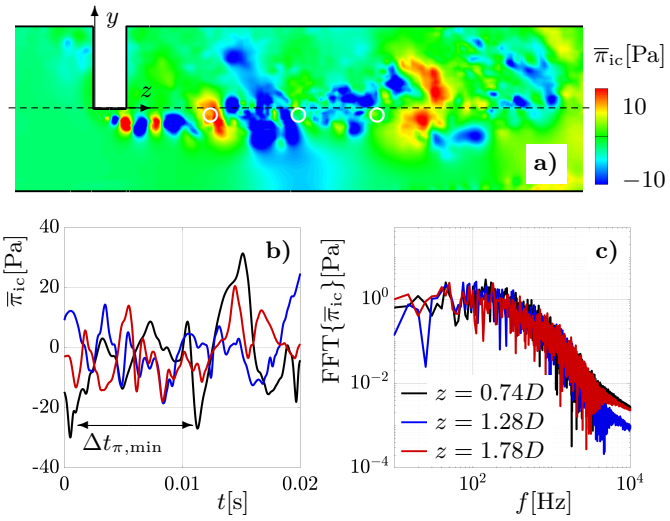

Figure 4: a) Contours of the instantaneous pseudo pressure fluctuation $\overline{\pi}_{ic}$, b) time signals at marked positions along $y = -0.05D$ line (white circles in a)), c) spectral representation.

as seen in figure 5 a. In consequence, the LES predicts very strong resolved Lighthill source terms in this region, as seen in figure 5 b. The SGS-contribution shown in figure 5 c is predicted one order of magnitude smaller than the resolved part. This is also confirmed by the spectra of the Lighthill source term, where the SGS-contribution is significant only at high frequencies associated with small spectral energy, as seen in figure 5 d.

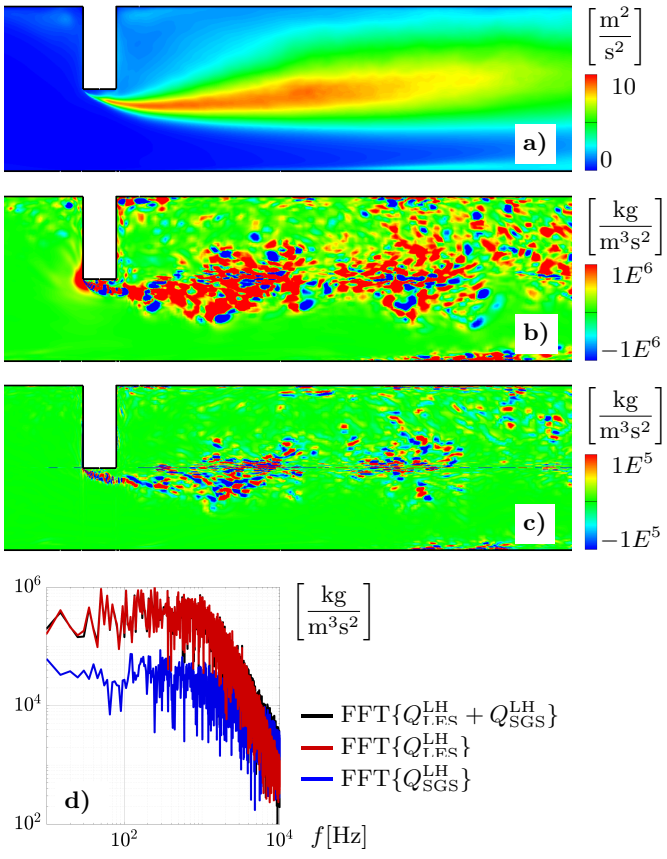

Figure 5: Contours of a) the resolved turbulent kinetic energy $\overline{k} = \overline{u}_i'\overline{u}_i'/2$, b) the resolved Lighthill source term Q^{LH}_{LES}, c) the SGS-contribution Q^{LH}_{SGS}. d) Spectral representations of the contributions at a selected point at $y = -0.05D$ and $z = 0.74D$, as marked in figure 4 a.

Figure 6 displays contours of the PCWE source term appearing on the rhs of equation (5), evaluated with the predicted pseudo pressure fluctuation $\overline{\pi}_{\mathrm{ic}} = \overline{\pi} - \langle\overline{\pi}\rangle$, such that

$$Q^{\mathrm{PCWE}} = \frac{D\overline{\pi}_{\mathrm{ic}}}{Dt} = \frac{\partial\overline{\pi}_{\mathrm{ic}}}{\partial t} + \langle u_j\rangle \frac{\partial\overline{\pi}_{\mathrm{ic}}}{\partial x_j}. \qquad (12)$$

The contours clearly reflect the vortex shedding downstream of the orifice. The transient part of the PCWE source term displayed in figure 6 b is equally strong throughout the shear layer. The convective component, shown in figure 6 c, contributes and even becomes dominant mainly on the lower side of the shear layer, where the axial velocity is very high.

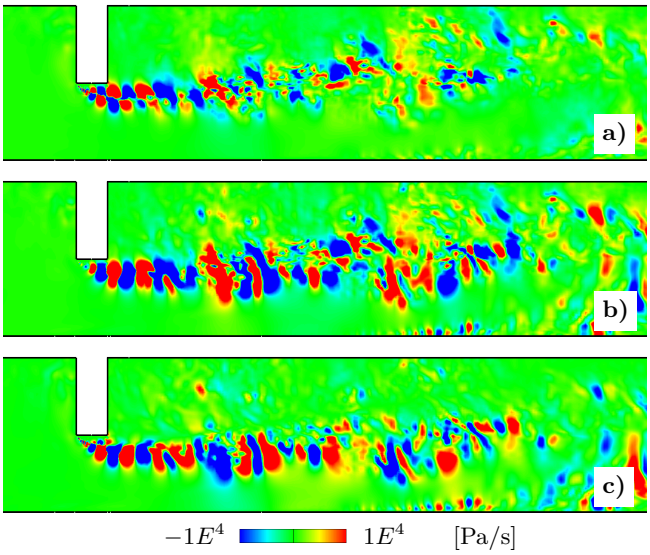

Figure 6: Contours of the PCWE source term: a) full term $Q^{\mathrm{PCWE}} = D\overline{\pi}_{\mathrm{ic}}/Dt$, b) transient component $Q^{\mathrm{PCWE}}_{\mathrm{dt}} = \partial\overline{\pi}_{\mathrm{ic}}/\partial t$, c) convective component $Q^{\mathrm{PCWE}}_{\mathrm{C}} = \langle\overline{u}_j\rangle\, \partial\overline{\pi}_{\mathrm{ic}}/\partial x_j$.

Comparison against measurements

For a validation of the present LES, the predicted pseudo pressure signals were compared against pressure signals measured by [5] in dedicated experiments, studying the same flow configuration in figure 7. In these experiments, near-wall pressure signals were measured using highly sensitive "Kulite" probes (K1 to K4) at selected positions up- and downstream of the orifice, as sketched in figure 7 a. As seen from the spectral distributions in figures 7 b-e, the predictions of the LES are in very good agreement with the measured spectra, down to the measuring limit of the Kulites.

Summary

The present study computationally investigates the aeroacoustic source terms generated in turbulent flow through a pipe with an orifice. The analysis is based on a hybrid approach, where an incompressible LES of the flow field is performed to predict instantaneous source terms for use in Lighthill's acoustic analogy and the PCWE. The modelled SGS-contribution turned out to contribute comparatively little to the Lighthill source term, adding mainly in the high-frequency range. Vortex shedding from the sharp upstream corner of the orifice

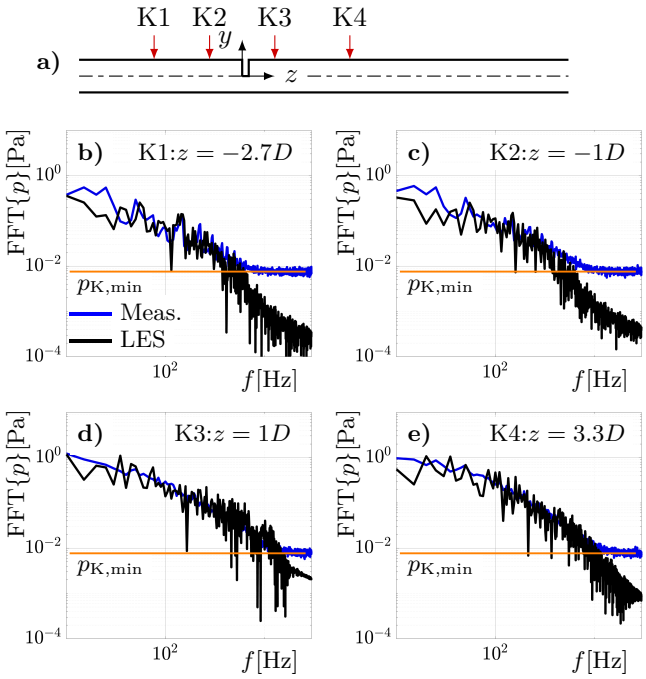

Figure 7: a) positions of Kulites, b)-e) spectra of predicted pseudo pressure compared against measurments at selected wall positions. The orange line indicates the lower measuring limit of the Kulites.

is identified as the dominant phenomenon for the generation of intense aeroacoustic sources, which is specially reflected by the PCWE source terms. For the validation of the LES, the predictions for the resolved pressure fluctuations were compared against experimental data. The observed good agreement in the pressure spectra qualifies the present LES as a suitable approach for computing flow-induced sound sources as a reliable input into acoustic wave equations.

References

[1] Curl, N.: The influence of solid boundaries upon aerodynamic sound. J. Proc. Roy. Soc. London (1955), 231-505

[2] Kaltenbacher, M. et. al.: Computational Aeroacoustics for Rotating Systems with Application to an Axial Fan. AIAA Journal (2017), 5

[3] Kobayashi, H.: The subgrid-scale models based on coherent structures for rotating homogeneous turbulence and turbulent channel flow. Physics of Fluids (2005), 17:045104

[4] Spazzini et. al.: Unsteady behavior of back-facing step flow. Experiments in Fluids (2001), 30:551-561

[5] Maurerlehner P. et. al.: Validation setup for the investigation of aeroacoustic and vibroacoustic sound emission of confined turbulent flows. Inter-Noise Conference, Washington (2021)